PLA2G6 guards placental trophoblasts against ferroptotic injury

Ofer Beharier[a], Vladimir A. Tyurin[b], Julie P. Goff[a], Jennifer Guerrero-Santoro[a], Kazuhiro Kajiwara[a], Tianjiao Chu[a], Yulia Y. Tyurina[a], Claudette M. St Croix[c], Callen T. Wallace[c], Samuel Parry[d], W. Tony Parks[e], Valerian E. Kagan[b], and Yoel Sadovsky[a,f,1]

[a]Magee-Womens Research Institute, Department of Obstetrics, Gynecology, and Reproductive Sciences, University of Pittsburgh, Pittsburgh, PA 15213; [b]Department of Environmental and Occupational Health and Center for Free Radical and Antioxidant Health, University of Pittsburgh, Pittsburgh, PA 15261; [c]Department of Cell Biology, University of Pittsburgh, Pittsburgh, PA 15261; [d]Department of Obstetrics and Gynecology, University of Pennsylvania School of Medicine, Philadelphia, PA 19104; [e]Department of Laboratory Medicine and Pathobiology, Mount Sinai Hospital, University of Toronto, Toronto, ON, Canada M5G 1X8; and [f]Department of Microbiology and Molecular Genetics, University of Pittsburgh, Pittsburgh, PA 15219

Edited by R. Michael Roberts, University of Missouri, Columbia, MO, and approved September 8, 2020 (received for review May 12, 2020)

The recently identified ferroptotic cell death is characterized by excessive accumulation of hydroperoxy-arachidonoyl (C20:4)- or adrenoyl (C22:4)- phosphatidylethanolamine (Hp-PE). The selenium-dependent glutathione peroxidase 4 (GPX4) inhibits ferroptosis, converting unstable ferroptotic lipid hydroperoxides to nontoxic lipid alcohols in a tissue-specific manner. While placental oxidative stress and lipotoxicity are hallmarks of placental dysfunction, the possible role of ferroptosis in placental dysfunction is largely unknown. We found that spontaneous preterm birth is associated with ferroptosis and that inhibition of GPX4 causes ferroptotic injury in primary human trophoblasts and during mouse pregnancy. Importantly, we uncovered a role for the phospholipase PLA2G6 (PNPLA9, iPLA2beta), known to metabolize Hp-PE to lyso-PE and oxidized fatty acid, in mitigating ferroptosis induced by GPX4 inhibition in vitro or by hypoxia/reoxygenation injury in vivo. Together, we identified ferroptosis signaling in the human and mouse placenta, established a role for PLA2G6 in attenuating trophoblastic ferroptosis, and provided mechanistic insights into the ill-defined placental lipotoxicity that may inspire PLA2G6-targeted therapeutic strategies.

ferroptosis | PLA2G6 | GPX4 | placenta | trophoblast

Unrestricted lipid peroxidation jeopardizes membrane structure, fluidity, and permeability, and may lead to cell injury or death (1, 2). This injury can be mitigated by antioxidant enzymes, including superoxide dismutase, catalase, thioredoxin, peroxiredoxin, and glutathione peroxidase (GPX) (3). Distinctively, ferroptosis is a recently identified form of lipoxygenase (LOX)-regulated, nonapoptotic cell death, characterized by iron-dependent accumulation of oxygenated phospholipids and relative insufficiency of glutathione peroxidase 4 (GPX4) (4–7). Considering hydroperoxide phospholipids, ferroptosis is characterized by the accumulation of hydroperoxide phosphatidylethanolamines (Hp-PEs) with preference to the fatty acyls arachidonoyl (termed HpETE-PE) and adrenoyl (termed HpDTE-PE) (4). Advanced liquid chromatography–mass spectrometry (LC-MS)-based redox phospholipidomics demonstrated that oxidation by 15-lipoxygenase (15-LOX), when coupled by PE-binding protein 1 (PEBP1), generates the pro-ferroptotic 15-HpETE-PE and 17-HpDTE-PE (4, 8–10). Recently, FSP1 was identified as a vital element of a nonmitochondrial CoQ antioxidant system that acts in parallel to the canonical glutathione-based GPX4 pathway (11, 12).

The placenta forms the maternal–fetal interface and plays a vital role in gas, nutrients, and waste exchange, the production of pregnancy hormones, and immune and mechanical defense of the developing fetus (13). These crucial functions are mediated primarily by trophoblasts that cover the entire villous surface of the placenta (14). Importantly, circumstances that have been previously implicated in ferroptosis are associated with placental physiology and pathobiology: 1) akin to processes that define ferroptosis in acute renal failure, asthma, neurotoxicity, cancer, and brain ischemia–reperfusion injury (7, 10, 15–17), the placenta is subject to hypoxia/reperfusion during the normal establishment of placental blood flow and the transition from histotrophic to hemotrophic placental support (18, 19) and later in pregnancy, during uterine contractions before or during labor (20, 21); 2) hypoxia/reperfusion injury has been implicated in the pathogenesis of placental dysfunction underlying preeclampsia, preterm birth, and fetal growth restriction (15, 22, 23); 3) iron, which is required for lipid peroxidation (24), is abundant in placental trophoblasts (25); 4) cellular lipid peroxidation has been described in placental injury (16, 26); and 5) *GPX4* mutations or lower GPX4 levels have been associated with human placental dysfunction and preeclampsia (24, 27–29) and inhibitors of ferroptosis-attenuated preeclampsia like symptoms in a rat model (29). These observations underscore the need to further investigate trophoblast ferroptosis and its role in placental injury underlying obstetrical syndromes. Notably, when compared to preeclampsia and fetal growth restriction (FGR), the placental pathobiological pathways causing spontaneous preterm birth (SPTB) and placental injury are less clear. Yet, uterine

Significance

Placental dysfunction has been causally linked to major pregnancy complications that are implicated in maternal–fetal morbidity and mortality, but the mechanisms underlying placental dysfunction are largely unknown. The recently identified ferroptotic cell death is characterized by excessive accumulation of hydroperoxide phosphatidylethanolamines. While oxidative damage commonly defines placental dysfunction, the role of ferroptosis in this process is largely unknown. We found that preterm birth is associated with ferroptotic signals, and that inhibition of GPX4, which converts unstable lipid hydroperoxides to nontoxic lipid alcohols, causes ferroptotic injury in primary human trophoblasts and in mouse pregnancy. Importantly, we found that the phospholipase PLA2G6 mitigates trophoblast and placental ferroptosis. Together, we identified placental ferroptosis and established a role for PLA2G6 in attenuating ferroptosis.

Author contributions: O.B., V.E.K., and Y.S. designed research; O.B., V.A.T., J.P.G., J.G.-S., K.K., C.M.S.C., C.T.W., and S.P. performed research; O.B., V.A.T., T.C., Y.Y.T., C.M.S.C., W.T.P., V.E.K., and Y.S. analyzed data; O.B., V.E.K., and Y.S. wrote the paper; V.A.T. and Y.Y.T. performed lipidomics analysis; C.M.S.C. analyzed cell images; and W.T.P. examined placenta pathology.

Competing interest statement: Y.S. is a consultant to Illumina, Inc.

This article is a PNAS Direct Submission.

[1]To whom correspondence may be addressed. Email: ysadovsky@mwri.magee.edu.

This article contains supporting information online at https://www.pnas.org/lookup/suppl/doi:10.1073/pnas.2009201117/-/DCSupplemental.

First published October 21, 2020.

contractions, the hallmark of SPTB, are associated with placental hypoxia/reoxygenation (H/R), a risk factor for ferroptosis. An increased level of lipid mediators and relevant enzymes, such as PTGS2 (COX2), are associated with ferroptosis (30) and have been implicated in the production of bioactive lipids that stimulate uterine contractions (31).

The phospholipase A2 (PLA2) protein family is a group of lipid-modifying enzymes. Within this family, the Ca-independent PLA2 protein, PLA2G6 (PNPLA9, iPLA2beta), is expressed in the human placenta (32). PLA2G6 hydrolyzes the second carbon chain of membrane phospholipids (33), a pivotal step in prostaglandin production (34, 35). Importantly PLA2G6 also hydrolyzes Hp-PE species that are implicated in ferroptosis (36–39). Mutations in PLA2G6 have been associated with Parkinson's disease, neurodegenerative disorders, and iron accumulation in the brain (34), reviewed in ref. 40. We therefore hypothesized that PLA2G6 activity mitigates ferroptosis, paralleling the GPX4-mediated defense mechanism. Here we demonstrate that: 1) SPTB in humans that is associated with injured placentas exhibits increased levels of Hp-PE, consistent with placental ferroptosis; 2) genetic and pharmacologic inhibition of GPX4 induces ferroptosis in human placental trophoblasts; 3) sublethal activation of ferroptosis signaling leads to cellular trophoblast dysfunction; 4) *PLA2G6*-deficient trophoblasts exhibit enhanced sensitivity to ferroptosis; and 5) *Pl2g6* deficiency sensitizes the mouse pregnancy to placental ferroptosis, accompanied by a higher risk of fetal demise.

Results

Human Placenta and Placental Trophoblasts Exhibit Ferroptosis. We first sought to determine whether ferroptosis is enhanced in human placentas from pregnancies complicated by SPTB and associated with placental injury when compared to gestational age-matched controls (preterm control, *SI Appendix*, Table S1). Using two independent experiments (Fig. 1 *A* and *B*) we found that the levels of Hp-PE products that are characteristic of ferroptosis were elevated in these placentas, compared to gestational age-matched controls. Similar results were observed with respect to 4-hydroxynonenal (4-HNE), a byproduct of lipid peroxidation (41) (*SI Appendix*, Fig. S1 *C* and *D*). Because the iron-rich trophoblasts, which are bathed in maternal blood, are directly subject to altered perfusion or oxygenation, we tested whether trophoblasts are sensitive to ferroptotic signals. Using the selective GPX4 inhibitor RSL3, we found that both primary human trophoblasts (PHT cells) or the human trophoblast line BeWo are sensitive to RSL3-dependent proferroptosis stimulation (42) (Fig. 1 *C* and *D* and *SI Appendix*, Fig. S2). Silencing *GPX4* confirmed trophoblast sensitivity to ferroptosis stimulation (Fig. 1*E*). Ferrostatin-1, a specific inhibitor of ferroptosis, but not inhibitors of apoptosis (zVAD-fmk) or necroptosis (necrostatin-1, necrostatin-1S) (43) eliminated RSL3-induced death (Fig. 1 *C* and *D* and *SI Appendix*, Fig. S2 *A–C*). As demonstrated in other cell types (37), trophoblast ferroptosis was blocked by the iron chelator deferoxamine (DFO) (*SI Appendix*, Fig. S2*C*). Together, these findings demonstrate that human placental trophoblasts are sensitive to ferroptosis.

Sublethal Activation of Ferroptosis Hinders Trophoblast Differentiation. Since the pathophysiology underlying placental dysfunction may affect trophoblast differentiation, we assessed the impact of sublethal activation of ferroptosis on trophoblasts (44). We performed LC-MS-based analysis of phospholipids in PHT cells exposed to low levels (50 nM, Fig. 1*C* and *SI Appendix*, Fig. S2*A*) of RSL3. We found that this stimulation led to accumulation of the characteristic proferroptotic oxidized lipids PE (18:0/20:4+2[0]) (4), which was inhibitable by ferrostatin-1 (Fig. 2 *A–C*). We therefore sought to determine whether sublethal stimulation of ferroptosis leads to trophoblastic dysfunction. Notably, trophoblast differentiation is characterized by fusion of mononucleated cytotrophoblasts to form multinucleated syncytiotrophoblasts, a process that is inducible by cAMP or protein kinase A (PKA) activation and is associated with enhanced production of human CGβ (hCGb) and human placental lactogen (hPL) glycoproteins (45). We found that low-dose RSL3 (25 to 50 nM) reduced the release of hCG and hPL from PHT cells, and this effect was mitigated by ferrostatin-1 (Fig. 2*D*). To define the main cellular and molecular pathways that are impacted by sublethal activation of ferroptosis, we activated ferroptosis in BeWo cells by *GPX4* silencing (Fig. 2*E*) and assessed RNAseq-based transcriptome changes, using Ingenuity pathway analysis (IPA) for upstream regulator analysis (46). IPA predicted significant inhibition of cAMP, PKA, and forskolin signaling in response to sublethal ferroptosis activation, all essential signals for trophoblast differentiation and function (Fig. 2*F*) (45), with the highest rank cellular network changes shown in Fig. 2*G*. Together, these data suggest that accumulation of HpETE-PE at subferroptotic concentrations hinders trophoblast differentiation. Because cytotrophoblasts are more susceptible than syncytiotrophoblasts to hypoxic injury (47–50), we asked whether differentiation modulates trophoblast response to ferroptosis. Interestingly, we found that syncytiotrophoblasts were more susceptible than cytotrophoblasts to RSL3-induced ferroptotic death (*SI Appendix*, Fig. S3), suggesting that enhanced trophoblast differentiation may potentiate trophoblast ferroptotic damage.

PLA2G6 Deficiency Sensitizes Trophoblasts to Ferroptosis. PLA2G6 (PNPLA9, iPLA2beta) is the Ca-independent PLA2 that is ubiquitously expressed in human placental trophoblasts (Human Protein Atlas) (32) (*SI Appendix*, Fig. S4). PLA2G6 hydrolyzes the second carbon chain of membrane phospholipids and releases a free fatty acid (FA), usually polyunsaturated FA (PUFA) (33). When activated by oxidized phospholipids or other reactive oxygen species (ROS) (36), PLA2G6 can hydrolyze these Hp-PL species, including mitochondrial peroxidized cardiolipins (37–39). We therefore surmised that ablation of *PLA2G6* will render trophoblasts susceptible to ferroptosis. Whereas *PLA2G6* deficiency in BeWo cells had an insignificant effect in the absence of RSL3, it markedly potentiated RSL3-induced ferroptosis compared to wild-type (WT) cells exposed to RSL3 (Fig. 3*A*). Further, we exposed BeWo cells to (*S*)-bromoenol lactone [(S)-BEL], a chiral-specific suicidal substrate that selectively inhibits PLA2G6 (51), and found that, like *PLA2G6* deficiency, (S)-BEL sensitized BeWo cells to ferroptosis (Fig. 3*B*). In contrast, knockout (KO) of another member of the PNPLA lipase family of lipases (52), *PNPLA2* had no effect on RSL3- stimulated ferroptosis (Fig. 3*C*). To better define the interaction of PLA2G6 and GPX4, we silenced *GPX4* expression in WT and in *PLA2G6* KO BeWo cells and found that *PLA2G6* KO potentiated the effect of *GPX4* knockdown on ferroptotic death (Fig. 3*D*). Using Liperfluo, a fluorescent probe that detects lipid peroxides in live cells, we found a time-dependent increase in total fluorescence intensity or in the fraction of Liperfluo-positive cell surface in *PLA2G6* KO-*GPX4* knockdown cells compared to control (Fig. 3 *E* and *F* and *SI Appendix*, Fig. S5 and movie in *SI Appendix*, Fig. S6), providing further support for the role of PLA2G6 in guarding trophoblasts against ferroptosis. Notably, Liperfluo signal partly localized with the plasma membrane, suggesting a site for enhanced sensitivity to ferroptosis in trophoblasts (53).

To further ascertain the role of PLA2G6 in ferroptotic death, we used phospholipidomics to assess differences in Hp-PE species between WT and *PLA2G6* KO BeWo cells exposed to RSL3. As shown in Fig. 3*G*, *PLA2G6* KO BeWo cells exhibited a significant increase in 15-HpETE-PE species, characteristic of ferroptosis. Finally, we asked if trophoblast differentiation affected the expression of GPX4 or PLA2G6. We found that

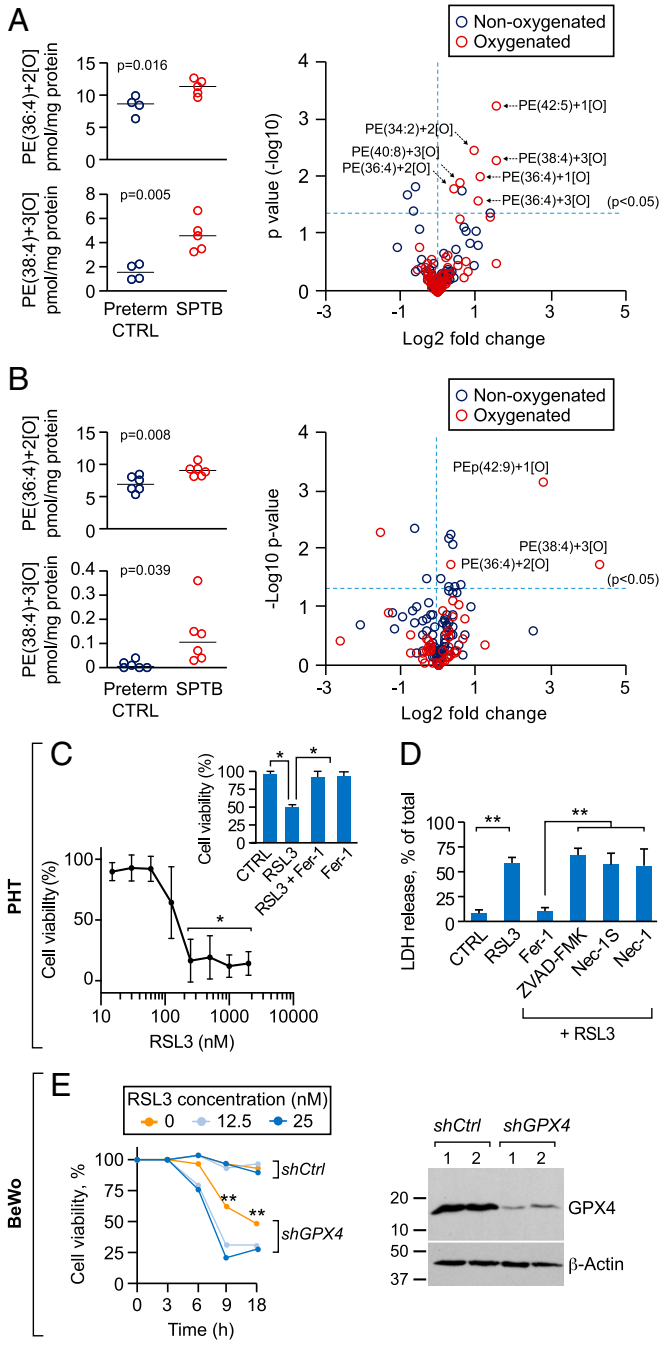

Fig. 1. Ferroptosis in human placentas from spontaneous preterm birth (SPTB) and in cultured human trophoblasts. (*A*–*B*) Two independent experiments (*A* and *B*) showing the levels of PE-((36:4)+2[O]) (16:0/20:4) and PE-((38:4)+3[O]) (18:0/20:4, *Left*), and volcano plots (*Right*) of placental oxygenated phospholipid species (red) vs. nonoxygenated (blue) in SPTB patients, compared to preterm controls (*A*, $n = 9$; *B*, $n = 12$). *P* values are shown in the panels, unpaired two-tailed *t* test. PE levels were determined by LC-MS as detailed in *Materials and Methods*. At *Left* each dot represents one placenta. Significant differences in Hp-PE species are depicted in the volcano plots as [–log10 (*P* value)] vs. [log2 (fold change)] by *t* test. (*C*) A concentration-dependent analysis of RSL3-induced cell death in PHT cells, measured by relative LDH release. Cell viability was calculated as 100% minus % released lactate dehydrogenase (LDH) of total cells. (*Inset*) Death (induced by 200 nM RSL3) was blocked by the ferroptosis inhibitor ferrostatin-1 (Fer-1, 0.5 μM). $*P < 0.01$ compared to the lowest concentration, LME model with Dunnett's method for multiple comparisons. (*Inset*) One-way ANOVA with Dunnett's method for multiple comparisons. (*D*) The effect of cell death inhibitors on RSL3-induced ferroptosis in PHT cells. Cells were exposed to RSL3 (200 nM, 24 h) in the absence or presence of ferroptosis inhibitor Fer-1 (0.5 μM), the pan-caspase inhibitor ZVAD-FMK (20 μM), the necroptosis inhibitors necrostatin-1S (Nec-1S, 50 μM), or necrostatin-1 (Nec-1, 50 μM). $**P < 0.01$, one-way ANOVA with Holm's method for multiple comparisons. (*E*) The viability of control BeWo (shCtrl) or *GPX4* knockdown BeWo cells (*shGPX4*), following Fer-1 withdrawal, with or without the addition of low-dose RSL3 (*Left*). Cell viability was calculated as 100% minus % released LDH of total cells. $**P < 0.01$, LME model with Holm's method for multiple comparisons. (*Right*) A representative immunoblot of silenced GPX4 expression. Data are presented as mean ± SD, $n = 4$ for different PHT cell batches for *C* and *D* and $n = 3$ for *E*.

differentiation of PHT cells is associated with reduced GPX4 expression and enhanced PLA2G6 expression (Fig. 3*H*), suggesting a compensatory protective role for PLA2G6 when the expression of GPX4 is reduced in differentiated trophoblasts.

Induction of Ferroptosis during Murine Pregnancy Triggers Fetal Demise. To examine the role of PLA2G6 in ferroptosis during pregnancy, we used the (1S,3R)-RSL3 isoform, previously shown to induce ferroptosis in vivo (54). Notably, up to 400 mg/kg of (1S,3R)-RSL3 was previously used, with no evidence of systemic toxicity (54), but with no data in pregnancy. We bred $Pla2g6^{Het}$ pairs and assessed pregnancy outcome following a low dose (25 to50 mg/kg) of (1S,3R)-RSL3, compared to control (Fig. 4*A*). We found that this dose was sufficient to increase placental Hp-PE levels (Fig. 4*B*) and caused dose-dependent fetal demise (Fig. 4*C*) with no effect on maternal lethality, weight (*SI Appendix*, Fig. S7*A*), or stress-related behaviors, including grooming, paw flinches and lifting, disorders of movement, or spontaneous standing. Moreover, using 25 mg/kg of (1S,3R)-RSL3, we did not detect an increase in injury-related transcripts or change in markers of ferroptosis and apoptosis in the kidney or liver of pregnant mice, when compared to vehicle-injected controls (*SI Appendix*, Fig. S7 *B*–*D*). Assessing ferroptosis activation in $Pla2g6^{WT}$ and $Pla2g6^{KO}$ pregnancies, we found that exposure to a low level (25 mg/kg) of (1S,3R)-RSL3 increased the mortality and resorption of $Pla2g6^{KO}$ embryos (Fig. 4 *D* and *E* and *SI Appendix*, Fig. S8), compared to $Pla2g6^{WT}$. Notably, survival and resorption were not affected by fetal sex (*SI Appendix*, Table S2). Among surviving pregnancies, the weight of $Pla2g6^{KO}$ embryos was lower than $Pla2g6^{WT}$ embryos, with no difference in placental weight between the different genotypes (*SI Appendix*, Fig. S8). However, in nonresorbed placentas, histological analysis revealed that the placental labyrinth of RSL3-exposed $Pla2g6^{KO}$ was thinner compared to $Pla2g6^{WT}$, while the junctional zone was unchanged (Fig. 4 *F* and *G*). Interestingly, administration of (1S,3R)-RSL3 had no effect on GPX4 or PLA2G6 expression (*SI Appendix*, Fig. S9), and the level of these enzymes was unchanged in placentals from SPTB (*SI Appendix*, Fig. S1 *A* and *B*).

Unlike the lethality of $Gpx4^{KO}$ murine embryos by embryonic day 8.5 (E8.5) (55), which precludes inferences about the role of GPX4 in placental function, $Pla2g6^{KO}$ pregnancies exhibit intact development in normal conditions. We therefore examined the role of PLA2G6 in H/R injury, a cause of placental dysfunction in pregnancy (15, 16, 22). We found that $Pla2g6^{KO}$ placentas exhibited accumulation of Hp-PE species that characterize ferroptosis (Fig. 5 *A* and *B*). As expected, H/R induced fetal growth restriction (Fig. 5*C*) with no difference in fetal or placental weight when only live fetuses were taken into account (Fig. 5 *C* and *D*). Importantly, feral demise was more common following H/R in $Pla2g6^{KO}$ pregnancies, when compared to $Pla2g6^{wt}$ (Fig. 5*E*), thus providing additional support for the role of PLA2G6 in protecting the fetoplacental unit against H/R injury.

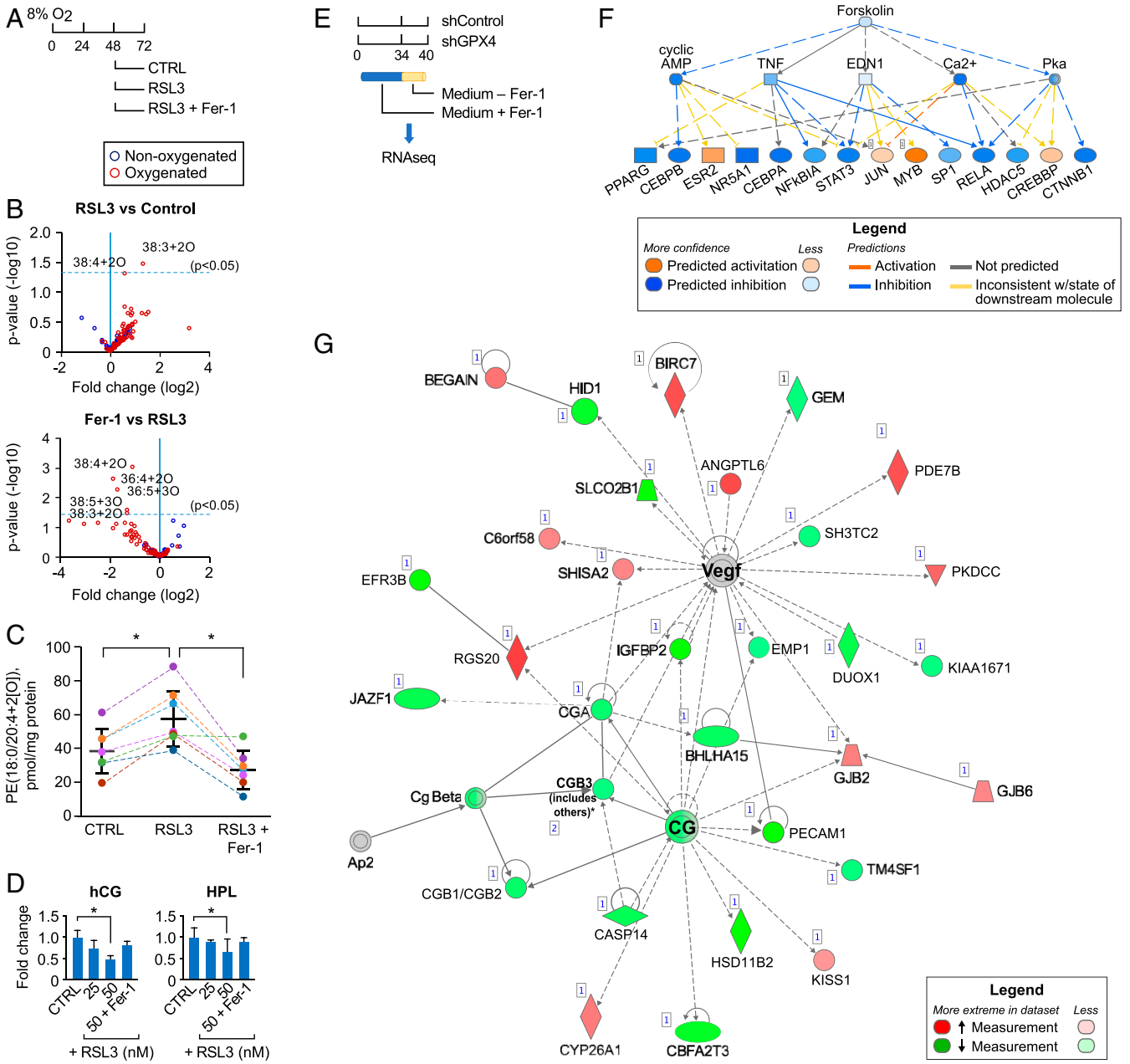

Fig. 2. Sublethal ferroptosis signaling impairs trophoblast function. (*A*) Scheme of ferroptosis signaling activation, using a low dose of RSL3 (50 nM) in PHT cells. (*B*) Volcano plots showing RSL3-induced changes in the levels of oxygenated (red) or nonoxygenated (blue) phospholipids in PHT cells, determined by LC-MS as detailed in *Materials and Methods*. The expression of Hp-PE species is shown as significance [–log10 (*P* value)] vs. [log2 (fold change)] by *t* test, in the absence (*Top*) or presence (*Bottom*) of ferrostatin-1 (Fer-1, 0.5 μM). $n = 6$ to 8 experiments. (*C*) The levels of PE-(C18:0/20:4+2[0]) in PHT cells exposed to DMSO, RSL3 (50 nM), or RSL3 + Fer-1 (0.5 μM, $n = 7$). $^*P < 0.01$, paired one-way ANOVA with Tukey's method for multiple comparisons. (*D*) The levels of hCG (*Left*) and hPL (*Right*) released from PHT cells 24 h after exposure to DMSO, RSL3 (50 nM), or RSL3 + Fer-1 (0.5 μM, $n = 5$). $^*P < 0.01$, LME model with Holm's method for multiple comparisons. (*E–G*) The effect of GPX4 silencing on upstream mechanistic network analysis, performed by IPA, as detailed in *Materials and Methods*. RNAseq was performed after silencing GPX4 in BeWo cells: *E* shows the experimental time course; *F* shows the predicted inhibition of cAMP, calcium, protein kinase A, and forskolin; and *G* depicts the cellular network most affected by sublethal ferroptosis activation and showing inhibition of key hormones and other markers of trophoblast differentiation and function. In *F* and *G*, the data were obtained from two independent experiments.

Discussion

Higher levels of oxidative stress with subsequent accumulation of ROS and lipid peroxidation have been commonly implicated in placental dysfunction (16) and related diseases (56–58), but the underlying damage pathways in these conditions remain largely unknown. Here we show that: 1) injured placentas associated with SPTB in humans exhibit increased levels of Hp-PE, consistent with placental ferroptosis; 2) placental trophoblasts require GPX4 activity for survival, as genetic and pharmacologic inhibition of GPX4 induces ferroptosis in placental trophoblasts; 3) sublethal activation of ferroptosis signaling leads to cellular dysfunction in trophoblast; 4) *PLA2G6*-deficient trophoblasts exhibit enhanced sensitivity to ferroptosis, which is augmented in the absence of GPX4 activity; and 5) while a low level of the GPX4 inhibitor (1S,3R)-RSL3 in pregnant mice did not lead to overt maternal toxicity, *Pl2g6* deficiency sensitizes the mouse

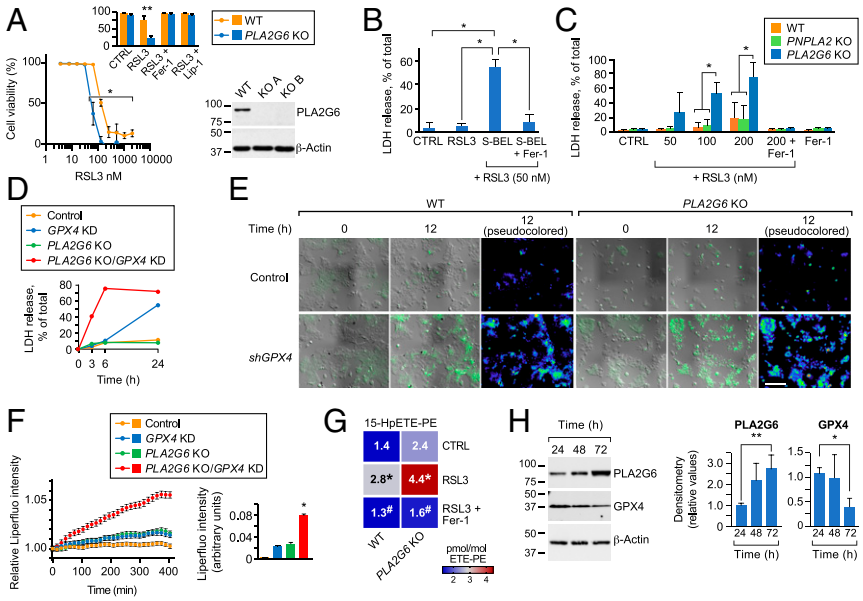

Fig. 3. Inhibition of PLA2G6 sensitizes trophoblasts to PE peroxidation and ferroptosis. (*A*) RSL3-induced concentration-dependent cell death of *PLA2G6*^{WT} and *PLA2G6*^{KO} BeWo cells. Cell viability was calculated as 100% minus % released LDH of total cells. *Inset*, death (induced by 100 nM RSL3) was blocked by the ferroptosis inhibitors ferrostatin-1 and liprostatin-1 (Fer-1 and Lip-1, 0.5 μM, respectively). *$P < 0.05$, LME model with Holm's method for multiple comparisons. *Inset*, LME model with Holm's method for multiple comparisons; **$P < 0.01$. Western blot represents KO efficiency of *PLA2G6*. (*B*) The effect of the PLA2G6 inhibitor, (*S*)-BEL, on RSL3-induced ferroptosis (24 h) and inhibited by Fer-1, as control. *$P < 0.05$, LME model with Dunnett's method for multiple comparisons. (*C*) The effect of increased concentration of RSL3 on ferroptosis in BeWo cells, sensitized by KO of the two PNPLA lipases, PLA2G6 (PNPLA9) or PNPLA2. Fer-1 (0.5 μM) inhibition was used as control. *$P < 0.05$, two-way ANOVA with interaction, with Holm's method for multiple comparisons. (*D*) Cell death induced after Fer-1 withdrawal from BeWo cells with either *GPX4*^{KD}, *PLA2G6*^{KO}, both *PLA2G6*^{KO}/*GPX4*^{KD}, or control. (*E*) Live cell fluorescence imaging of lipid hydroperoxides in the BeWo lines depicted in the figure, following withdrawal of Fer-1 (time 0 and 12 h). (*F*, *Left*) Fluorescence time course (relative to baseline) after Fer-1 withdrawal from BeWo cells with either *GPX4*^{KD}, *PLA2G6*^{KO}, both *PLA2G6*^{KO}/*GPX4*^{KD}, or control. (*F*, *Right*) Quantitative analysis of Liperfluo fluorescence intensity in *E*, at 12 h of experiment. *$P < 0.05$, one-way ANOVA with Tukey's method for multiple comparisons. Data are from a minimum of 10 stage positions. (*G*) LC-MS-based heat maps showing changes in 15-HpETE-PE in RSL3 (50 nM, 24 h)-exposed BeWo WT or *PLA2G6*^{KO} cells in the absence or presence of Fer-1. LC-MS data are normalized to parent species ETE-PE. Data represent pmol/mol 15-HpETE-PE (mean ± SD, $n = 3$). *$P < 0.001$ vs. control $^{\#}P < 0.002$ vs. RSL3 exposed cells, two-way ANOVA with Sidak's method for multiple comparisons. (*H*, *Left*) Representative western blot of GPX4, PLA2G6, and β-actin expression in PHT cells over time in culture. (*H*, *Right*) Densitometry analysis of GPX4 and PLA2G6 expression over time in culture. $n = 4$, *$P < 0.05$, **$P < 0.001$, comparing each measurement at 48 h or 72 h against 24 h. LME model with Dunnett's method for multiple comparisons.

pregnancy to placental ferroptosis, accompanied by increased incidence of fetal demise.

Imai et al. (55) previously showed that *Gpx4*^{KO} mouse embryos did not survive beyond E8.5, a time point of chorioallantoic villi formation (59), thus precluding any inferences about the role of GPX4 in placental development and function. Our study design allowed us to uncover the critical role of active antiferroptotic machinery for fetoplacental survival and pregnancy outcome. Consistent with our data are the findings of low levels of GPX4 expression in dysfunctional placentas from pregnancies with preeclampsia (28), and a higher risk for preeclampsia in patients with mutations in *GPX4* (27).

Ferroptosis occurs when the level of Hp-PE exceeds cellular defense, reaching a critical level that has been described as "ferroptotic threshold" (44). Our report directly links ferroptotic Hp-PE signals to human placental dysfunction and is consistent with the previously reported elevated levels of malondialdehyde (MDA) and 4-HNE, products of lipid peroxidation, in human placental dysfunction (60–63). We discovered that sublethal activation of proferroptotic signaling below the ferroptotic death threshold impairs distinct trophoblast differentiation pathways and thus enhances placental dysfunction. Our findings of elevated levels of Hp-PE, combined with evidence of lipotoxic injury in SPTB placentas compared to preterm control, highlight the significance of ferroptotic dysfunction in placental pathophysiology, likely relevant to injury in other tissues (64, 65).

We demonstrated that, at baseline and in the presence of intact GPX4, deletion of *PLA2G6* was not sufficient to induce ferroptosis, implying that PLA2G6 provides a secondary line of defense against ferroptosis, which may be particularly important when the potent action of GPX4 is exhausted (Fig. 5*F*) (66–69). Data derived from experiments in nonplacental tissue show that PLA2G6 hydrolyzes Hp-PE into lyso-PE and oxidized FA (36–39). Thus, PLA2G6 may act in concert with a known ferroptosis-regulating enzyme, lysophosphatidylcholine acyltransferase 3 (LPCAT3) (70) to convert proferroptotic signals into "healthy" membrane phospholipids. Indeed, observation by others regarding significant accumulation of Hp-PE in mice with deficiency or function-perturbing mutation of PLA2G6 (71, 72) bolsters our observation regarding the pivotal role of this enzyme in metabolizing HpETE-PE and HpDTE-PE and thereby eliminating the ferroptotic signal. Our data reveal that PLA2G6 is central for trophoblast defense against ferroptosis and placental injury. Nevertheless, the importance and impact of other modulators of ferroptosis (ALOX15, PEBP1, ACSL4, ACAT, FSP1, cytochrome P450 oxidoreductase, TFR1, ferritin, Nrf2, HMOX1, and prominin 2) (42, 73–75) on trophoblast function remain to be established. In addition, we did not address the possibility that PLA2G6 may affect the cellular distribution of Hp-PE or other lipotoxic signals (53). Our findings suggest that ferroptosis-inhibiting agents may broaden the therapeutic strategies in diseases that stem from lipotoxic tissue injury, such as placental dysfunction that manifest as SPTB, preeclampsia, or fetal growth restriction.

Materials and Methods

Placental Sample Collection, Trophoblast Culture, and Ligands. All participants provided written informed consent to the use of placental biopsies, under a

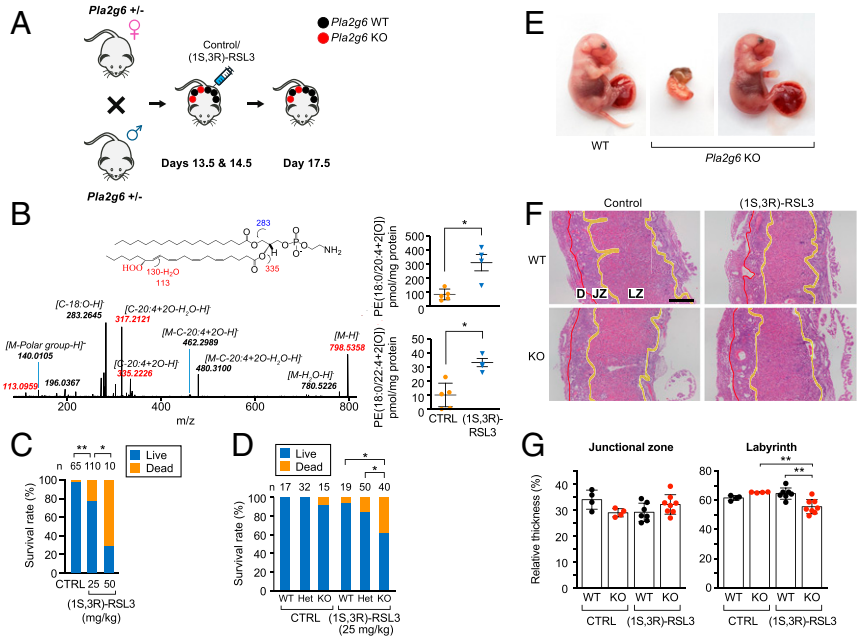

Fig. 4. *Pla2g6* deficiency triggers ferroptosis during murine pregnancy. (*A*) Schematic of the breeding strategy, embryo/placenta genotypes, and the timing of i.p. injection of vehicle or (1S, 3R)-RSL3. (*B*) Accumulation of ferroptotic Hp-PE species in the WT placentas, harvested at E17.5, following i.p. injection of vehicle control or 25 mg/kg of (1S, 3R)-RSL3 at E13.5 and E14.5. Control, $n = 5$; (1S, 3R)-RSL3, $n = 4$. The data are quantified next to the LC-MS result. $*P < 0.05$, unpaired two-tailed *t* test. (*C*) Fetal survival (all genotypes), assessed at E17.5 after injection of vehicle (1S, 3R)-RSL3, as shown in *A*. The number of embryos in each group is indicated above each bar. $*P < 0.05$, $**P < 0.01$, Fisher's exact test with Holm's method for multiple comparisons. (*D*) Fetal survival at E17.5 after injection of vehicle or (1S, 3R)-RSL3 (25 mg/kg) at E13.5 and E14.5, analyzed by embryo *PLA2G6* genotype. The number of embryos in each group is indicated above each bar. $*P < 0.05$, Fisher's exact test with Holm's method for multiple comparisons. (*E*) Photos of representative placenta and embryo from E17.5 of *Pla2g6*^{WT} and *Pla2g6*^{KO} injected with (1S, 3R)-RSL3 (25 mg/kg) as shown in *A*. Surviving embryos (*Right*) did not exhibit overt malformations. (*F*) Representative low magnification images of H&E-stained placentas (sagittal section), showing the labyrinth zone (LZ), junctional zone (JZ), and decidua (D). (Scale bar, 500 μm.) (*G*) Quantification of the placental layers in *F*, expressed as width compared to the total placental thickness (WT, $n = 4$ and 7 placentas from 2 and 3 litters, for vehicle and (1S, 3R)-RSL3, respectively; KO, $n = 4$ and 8 placentas from 2 and 5 litters, for vehicle and (1S, 3R)-RSL3, respectively). $**P < 0.01$, two-way ANOVA with interaction, with Holm's method for multiple comparisons.

protocol approved by the institutional review board (IRB) at the University of Pittsburgh (STUDY19120076). PHT cells were isolated from healthy singleton term placentas under an exempt protocol approved by the University of Pittsburgh's IRB (PRO08030033). Upon admission to the hospital, patients provided written informed consent for the use of deidentified and discarded tissues for research. Placental biopsies (5 mm^3) were obtained immediately after delivery, using a region of the placenta that is midway between the cord insertion and the placental margin and between the chorionic and basal plates, as we previously detailed (76). Biopsies from the same site were 1) snap frozen in liquid nitrogen within 30 min of delivery and stored in −80 °C until processed for phospholipid content, as we detail below and 2) used for paraffin embedding (see below).

PHT cells were prepared from term human placentas after uncomplicated labor and delivery using the trypsin-DNase-dispase/Percoll method, as previously described (77), with modifications (49, 78). Isolated PHT cells (350,000 cells/cm^2) were cultured for 24 to 96 h in 8% O_2 5% CO_2, at 37 °C, thus recapitulating O_2 concentrations in the intervillous space after the first trimester of human pregnancy, when the intervillous space is fully perfused by maternal blood (79, 80), using Dulbecco's Modified Eagle's Medium (DMEM) (Sigma-Aldrich) supplemented with 10% fetal bovine serum (Sigma-Aldrich) and 1% antibiotics. To limit differentiation, PHT cells were cultured in Ham/Waymouth medium, composed of equal volumes of Ham F12 and Waymouth medium (Gibco) (49). For assessment of ferroptosis, PHT cells were seeded in a 6-well plate and exposed to different concentrations of RSL3 (S8155, Selleck Chemicals) for 24 h. The BeWo trophoblast cells (ATCC, CCL-98) were maintained in F12K Kaighn's modified medium (Gibco) supplemented with 10% bovine growth serum (HyClone) and antibiotics. For induction of ferroptosis, the cells were seeded at 180,000/well in a 12-well plate. After 24 h, the cells were exposed to RSL3, with or without ferrostatin-1 (Fer-1, S7243, Selleck Chemicals); liproxstatin-1 (S7699, Selleck Chemicals); Nec-1 (2324, Tocris); Nec-1s (2263-1, BioVision); Z-VAD-FMK (260138, Enzo Life); or DFO (138147, Sigma-Aldrich). Induction of ferroptosis in BeWo cells was performed in serum-free medium. Note that in experiments targeting the induction of ferroptosis, all cells were maintained in Fer-1-containing medium, to avoid the premature activation of ferroptosis in cells devoid of GPX4 or PLA2G6. The medium was washed and changed to Fer-1-free medium at the start of the experiment. Where indicated, the PLA2G6 inhibitor (*S*)-BEL (10 μM, 222281A, Santa Cruz) was added for 30 min in serum-free medium at 37 °C. The cells were then washed before exposure to RSL3 in the presence or absence of ferrostatin.

Cell Death Assay. Cell death was measured using the lactate dehydrogenase-based CytoTox-ONE homogeneous membrane integrity assay (Promega) according to the manufacturer's instructions. Sample fluorescence was measured at 560 nm excitation and 590 nm emission using a fluorescence microplate reader (SpectraMax Gemini EM, Molecular Devices).

ELISAs. For analyses of hormone release, cell culture supernatants were collected, and enzyme immunoassay was performed for either hCG (Abnova) or hPL (DRG), following the manufacturer's instructions. Hormone release was matched and normalized per placenta, comparing RSL3 and RSL3 + ferrostatin-1 to control dimethyl sulfoxide (DMSO).

Histology and Immunofluorescence. Placentas were fixed with 4% paraformaldehyde (Thermo Fisher) in 0.1 M phosphate buffer solution (PBS) and embedded in paraffin. Sections (5 μm) were used for hematoxylin-eosin (H&E) staining and microscopic analysis of the junctional zone/labyrinth architecture. Layer width was analyzed using ImageJ and expressed as a proportion of total placental thickness. PLA2G6 was detected using anti-PLA2G6 rabbit polyclonal primary antibody (*SI Appendix*, Table S3). Following PBS/Tween washes, the slides were incubated with donkey anti-rabbit 594 secondary antibody (*SI Appendix*, Table S3) for 1 h, at room temperature. Additional details, including 4-HNE and terminal deoxynucleotidyl transferase dUTP nick end labeling (TUNEL) assays, are available in *SI Appendix*.

Western Immunoblotting, RNA Extraction, and RT-qPCR. Cells were washed twice with PBS and lysed. Placental biopsies were snap frozen as detailed above. The tissues were thawed and homogenized. Extracted proteins were

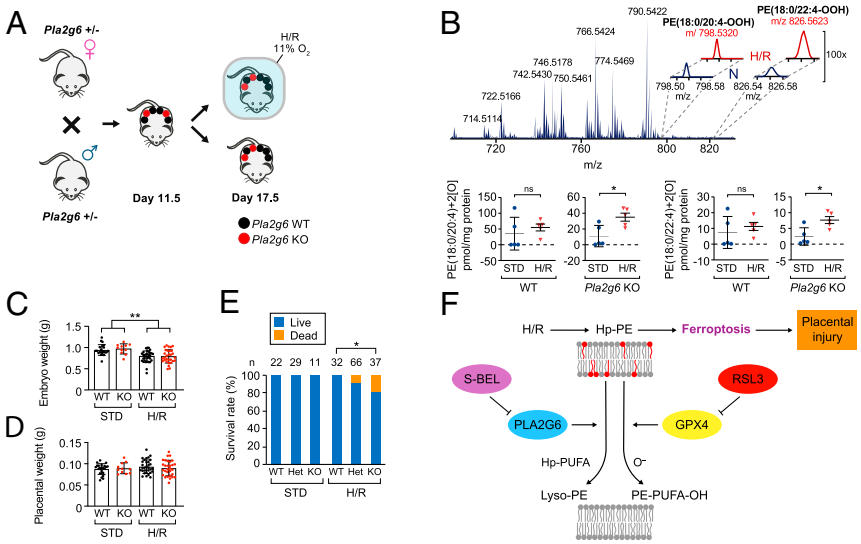

Fig. 5. *Pla2g6* expression attenuates placental ferroptosis induced by hypoxia/reoxygenation (H/R). (*A*) Schematic of the breeding strategy, embryo/placenta genotypes, and timing of H/R. (*B*) Accumulation of ferroptotic Hp-PE species in the placenta in response to H/R vs. standard (STD) conditions for $Pla2g6^{WT}$ (n = 4 placentas from three litters for STD and H/R) and $Pla2g^{KO}$ (n = 4 placentas from three litters for STD and H/R). The data are quantified below the LC-MS result. $*P < 0.05$, ns, not significant, unpaired two-tailed t test. (*C*) Embryo weights collected at E17.5 from $Pla2g^{KO}$ (n = 11 or 37 embryos for standard conditions (STD) or H/R, respectively) and from $Pla2g6^{WT}$ (n = 22 and 32 embryos for STD and H/R, respectively). $**P < 0.01$, two-way ANOVA, with Holm's correction for multiple comparisons. (*D*) Placental weights from the same embryos and conditions as in *C*. (*E*) Fetal survival (%) at E17.5 of $Pla2g6^{KO}$ vs. $Pla2g6^{WT}$ embryo, exposed to H/R or STD conditions. The number of embryos in each group is indicated above each bar. $*P < 0.05$, Fisher's exact test with Holm's method for multiple comparisons. The data are mean ± SD. (*F*) Schematic model, summarizing the role of PLA2G6 in attenuating ferroptosis signaling and placental injury.

separated by sodium dodecyl sulfate–polyacrylamide gel-electrophoresis (SDS/PAGE) and transferred to polyvinylidene difluoride membranes (Bio-Rad) as previously described (81). Blots were blocked and incubated overnight at 4 °C with antibodies against GPX4, PLA2G6, 15-LOX, ACSL4, PEBP, or actin (*SI Appendix*, Table S3), then incubated with goat anti-mouse HRP-conjugated secondary antibody. RNA extraction and RT-qPCR were performed using standard procedures. Additional details, including 4-HNE and TUNEL assays, are available in *SI Appendix*.

Phospholipidomics. Lipids were extracted by the Folch procedure (82), with slight modifications, with all steps under nitrogen atmosphere. Lipid phosphorus was determined by a micromethod (83). Liquid chromatography/electrospray ionization-mass spectrometry (LC/ESI-MS) analysis of lipids was performed on a Dionex HPLC system (utilizing Chromeleon software), consisting of a Dionex UltiMate 3000 mobile phase pump equipped with an UltiMate 3000 degassing unit and UltiMate 3000 autosampler (sampler chamber was set at 4 °C). The Dionex HPLC system was coupled to an Orbitrap Fusion Lumos mass spectrometer or on a Q-Exactive Hybrid Quadrupole-Orbitrap mass spectrometer (both from Thermo Fisher). Phospholipids were separated on a normal phase column (Luna 3 μm Silica2 100 A, 150 × 1.0 mm, Phenomenex) at a flow rate of 0.05 mL/min. The column was maintained at 35 °C. The analysis was performed using gradient solvents (A and B) containing 10 mM ammonium format. Solvent A contained propanol:hexane:water (285:215:5, vol/vol/v) and solvent B contained propanol:hexane:water (285:215:40, vol/vol/v). The column was eluted for 0.5 min isocratically at 25% solvent B, then from 0.5 to 6.5 min with a linear gradient from 25 to 40% solvent B, from 6.5 to 25 min using a linear gradient from 40 to 55% solvent B, from 25 to 38 min with a linear gradient from 55 to 70% solvent B, from 38 to 48 min using a linear gradient from 70 to 100% solvent B, then isocratically from 48 to 55 min at 100% solvent B, followed by a return to initial conditions from 55 to 70 min from 100 to 25% solvent B. The column was then equilibrated at 25% solvent B for an additional 5 min. The Orbitrap Fusion Lumos mass spectrometer (Thermo Fisher) was operated with electrospray ionization probe in negative polarity mode. Ion source conditions were set as follows: spray voltage = 3 kV, sheath gas = 55 (arbitrary unit), auxiliary gas = 10 (arbitrary unit), sweep gas = 0.5 (arbitrary unit), transfer tube temperature = 300 °C, vaporizer temperature = 200 °C, and RF-lens level = 20%. Data were acquired in data dependant-MS2 targeted-MS3 mode with a cycle time setting of 3 s. For MS scan event, the parameters were set as follow: ion detection = Orbitrap, mass resolution = 120,000, scan range = *m/z* 400 to 1,800, and automatic gain control target = 1e5. The most intense ion was selected for the data-dependent MS2 scan. Dynamic exclusion = 9 sed. Exclusion mass list for MS2 (*m/z* values of 130 background ions) was created from solvent blank injection data. For MS2 scan event(s), the parameters were set as follows: quadrupole isolation = 1 Da, activation type = higher-energy collisional dissociation, collision energy = 28% with step 8%, ion detection = Orbitrap, mass resolution = 15,000, max injection time = 250 ms, and AGC target = 2e4. All organic solvents and other biochemical reagents were purchased from Sigma-Aldrich. One-hexadecanoyl(d31)-2-(9Z-octadecenoyl)-sn-glycero-3-phosphoethanolamine and 1-stearoyl-2-arachidonoyl-sn-glycero-3-phosphoethanolamine (SAPE) were purchased from Avanti Polar Lipids. The 1-Stearoyl-2-15(S)-HpETE-sn-glycero-3-phosphoethanolamine and 1-stearoyl-2-15(S)-HETE-sn-glycero-3-phosphoethanolamine were obtained from Cayman Chemical.

Lentivirus and shRNA-Mediated Silencing. Stable knockdown of *GPX4* expression in BeWo cells was performed using MISSION shRNA plasmids (Sigma-Aldrich). Lentiviral vectors (pLKO.1) encoding either a nontargeting shRNA (SHC016, Sigma-Aldrich) or shRNA directed against human GPX4 (TRCN0000046251, designated shGPX4, Sigma-Aldrich) were cotransfected with pMD2.G and psPAX2 plasmids (Addgene 12259, 12260, respectively) into the HEK293T packaging cell line, using TransIT-Lenti transfection reagent (Mirus). After 48 to 72 h, viral particles were harvested from the culture supernatant by filtering through a 0.45-μm syringe filter and concentrated by centrifugation (18,000 rpm for 2 h), aliquoted, and stored at −80 °C. Viral particles, harboring either nontargeting control or GPX4-directed shRNA, were used to transduce BeWo cells following polybrene (8 μg/mL, Sigma-Aldrich) for 1 h. After 48 h, transduced cells were selected with 2 μg/mL puromycin (Sigma-Aldrich). Ferrostatin-1 (0.5 μM) was added to inhibit spontaneous ferroptosis.

Generation of *PLA2G6* and *PNPLA2* KO BeWo Cells. HEK293T cells were transiently transfected with pMD2.G, psPAX2, and pCW-Cas9 (50661, Addgene) plasmids, using TransIT-Lenti transfection reagent (Mirus), and incubated to generate lentiviral particles. Supernatants carrying retroviruses were collected 48 h after transfection and used to infect BeWo cells, establishing the parental clone, which expresses high levels of Cas9 in response to doxycycline exposure. To target *PLA2G6* or *PNPLA2*, single-guide RNAs (sgRNAs) were selected, using the Massachusetts Institute of Technology CRISPR design tool (https://zlab.bio/guide-design-resources), as shown in *SI Appendix*, Table S4. The plasmid pLKO5.sgRNA.EFS.tRFP657 (57824, Addgene) was used

for the *PLA2G6* guide. The plasmid pLKO5.sgRNA.EFS.GFP (57822, Addgene) was used for the *PNPLA2* guide. Both plasmids were kindly provided by the Ebert Laboratory (Dana-Farber Cancer Institute, Boston, MA) (84), and their protocols were followed to anneal the primers containing the sgRNA and ligate them to the respective vectors. Lentiviruses were made, as described above, using a HEK293T cell packaging system, then used to infect the BeWo-doxycycline-inducible Cas9 cells. Cells were sorted by fluorescent signals (RFP and GFP for PLA2G6 and PNPLA2, respectively). The cell population exhibiting the highest signal was sorted to isolate single clones, which were PCR screened to identify the relevant genomic DNA indel. Knockout clones were also confirmed using western immunoblotting.

RNA Isolation, Library Construction, Sequencing, and Bioinformatic Analysis. For RNAseq, total RNA was isolated from two independent cell culture experiments, using TRIreagent (Thermo Fisher), and processed using the RNeasy mini kit (Qiagen), following the manufacturer's instructions. PolyA selection, reverse transcription, library construction, sequencing, and initial analysis were performed by Novogene. RNA libraries from BeWo-shControl and BeWo-shGPX4 samples were aligned to human reference genome GRCh38, using the RNAseq alignment tool STAR (85), and annotated with the latest GENCODE (86). The number of reads per gene was calculated for each RNAseq library, also using STAR. We used the median of ratios method implemented in the R package DESeq2 (87) to normalize the long RNA counts in the sequencing libraries. The log2 fold change of the normalized counts was used to rank the differentially expressed candidate genes and as input to the Ingenuity pathway analysis tool for the identification of the canonical pathways and functions associated with the differentially expressed candidate genes. RNAseq data were deposited in the National Center for Biotechnology Information's Gene Expression Omnibus (GEO, accession number GSE147625).

Transcriptome Pathway Analysis. To identify relevant biological pathways that are implicated in sublethal activation of ferroptotic signaling, we applied IPA methodology (IPA Software, Ingenuity Systems), which predicts upstream signaling pathway and protein networks. For input, we used our RNAseq of BeWo expressing shControl vs. shGPX4, following 6 h of ferrostatin-1 withdrawal. We performed IPA upstream mechanistic network analysis and cellular network analysis to characterize trophoblast response to sublethal ferroptotic activation.

Imaging of Intracellular Lipid Peroxidation. To visualize intracellular lipid peroxidation, BeWo cells (wild type, *shGPX*, *PLA2G6* KO, or both *shGPX* and *PLA2G6* KO) were seeded in a four-chamber glass-bottom tissue culture dish (35 mm, MatTek Corp). After 48 h, the cells were prestained with Liperfluo (10 μM, Dojindo Molecular Technologies) for 30 min, washed twice with PBS, and then cultured in ferrostatin-1-free medium. The dish was inserted into a closed, thermo-controlled (37 °C) stage top incubator (Tokai Hit Co.) above the motorized stage of an inverted Nikon TiE fluorescent microscope equipped with a 20× optic (Nikon, CFI Plan Fluor, NA 0.75). Liperfluo was excited using a diode-pumped light engine (SPECTRA X, Lumencor) and detected using an ORCA-Flash 4.0 sCMOS camera (Hamamatsu) and excitation and emission filters from Chroma. Data were collected every 15 min for 12 h, on ∼10 to 20 cells per stage position, with 10 to 15 stage positions in each of four separate experiments per condition. Data were collected and analyzed using NIS Elements (Nikon). Additional details on analysis of fluorescence signal propagation are available in *SI Appendix*.

Generation of *Pla2g6* KO Mice and Experimental Exposures In Vivo. All experiments using mice were approved by the Institutional Animal Care and Use Committee of Magee-Womens Research Institute and the University of Pittsburgh (protocol 19075519) and conducted in accordance with United States - Public Health Service policy, as defined in the Guide for the Care and Use of Laboratory Animals (88). *Pla2G6^{Het}* mice were obtained from The Jackson Laboratory. For timed breeding, *Pla2G6^{Het}* females were housed with *Pla2g6^{Het}* males overnight and separated the next day, defined as E0.5. All mice were kept under standard conditions of 14:10 h dark and light cycle and fed a regular rodent chow diet and water. Pregnancy was confirmed by a 10% weight gain by E11.5. On E13.5 and E14.5, pregnant dams were subjected to i.p. injection of 100 μL vehicle (DMSO) control or (1S,3R)-RSL3 (19288, Cayman), which was dissolved in DMSO (D8418, Sigma-Aldrich) and diluted in PBS:polyethylene glycol solution (202371, Sigma-Aldrich) to a final ratio of 25%, 37.5%, 37.5%, respectively. Dams were killed on E17.5, placentas and embryos were weighed, and placentas were fixed using 4% paraformaldehyde or frozen at −80 °C for lipidomic analysis and western blot until processed. Genotyping was performed by standard PCR (Verity, Applied Biosystems), using specific primer sets (*SI Appendix*, Table S5), following genomic DNA being isolated from fetal tail by the HotSHOT (hot sodium hydroxide and Tris) method, adapted from Truett et al. (89). Fetal sex determination was performed using standard PCR with specific primer set (*SI Appendix*, Table S5) for sex-determining region Y (SRY). Amplification products were visualized on agarose gel with 1% SYBR Safe (Invitrogen). Pregnant mice were kept in room air except that, in the H/R experiments, the mice were placed in a hypoxia chamber (Coy Laboratory Products) in an 11% O_2 atmosphere between E11.5 and E17.5. On E17.5, hypoxic mice were removed from the hypoxia chamber for a 4- to 12-h period of reoxygenation, killed, placentas and embryos were weighed, and placentas fixed using 4% paraformaldehyde, or frozen at −80 °C for lipidomic analysis and western immunoblotting.

Statistical Analysis. All of the noncount data were analyzed using either the linear models, in the form of one-way or two-way ANOVA and linear regression model, or using the linear mixed effect (LME) models when the observations were correlated. Fisher's exact test was performed on the count data to test the difference in ratios. For multiple comparisons, Holm's method (for arbitrarily selected comparisons), Dunnett's method (for multiple comparisons against a single control), or Tukey's method (for all pairwise comparison of every condition to every other condition) were used to control family-wise error rates. In some cases, *t* test was used, where appropriate. Data are presented as means ± SD where relevant. $P < 0.05$ was determined to be significant.

Data Availability. Anonymized (RNAseq) data have been deposited in National Center for Biotechnology Information (NCBI)'s Gene Expression Omnibus (GEO, Ofer Beharier, Sub-lethal stimulation of ferroptosis leads to trophoblast dysfunction, https://www.ncbi.nlm.nih.gov/geo/query/acc.cgi?acc=GSE147625, March 27, 2020).

Additional details of experimental methods are available in *SI Appendix*.

ACKNOWLEDGMENTS. We thank Elena Sadovsky, Tiffany Coon, and Huijie Sun for technical assistance; Lori Rideout for assistance with manuscript preparation; and Bruce Campbell for editing. The project was supported by Eunice Kennedy Shriver National Institute of Child Health and Human Development (NIH/NICHD) grant P01HD069316 (to Y.S.), the March of Dimes Prematurity Research Center at the University of Pennsylvania (to S.P. and Y.S.), the 25 Club of Magee-Womens Hospital (to Y.S.), a Magee-Womens Research Institute Postdoctoral Fellowship (to O.B.), and the Jikei University School of Medicine Department of Obstetrics and Gynecology (to K.K.).

1. L. Ung *et al*., Oxidative stress and reactive oxygen species: A review of their role in ocular disease. *Clin. Sci. (Lond.)* **131**, 2865–2883 (2017).
2. A. Catalá, M. Díaz, Editorial: Impact of lipid peroxidation on the physiology and pathophysiology of cell membranes. *Front. Physiol.* **7**, 423 (2016).
3. X. Ren *et al*., Redox signaling mediated by thioredoxin and glutathione systems in the central nervous system. *Antioxid. Redox Signal.* **27**, 989–1010 (2017).
4. V. E. Kagan *et al*., Oxidized arachidonic and adrenic PEs navigate cells to ferroptosis. *Nat. Chem. Biol.* **13**, 81–90 (2017).
5. S. J. Dixon *et al*., Ferroptosis: An iron-dependent form of nonapoptotic cell death. *Cell* **149**, 1060–1072 (2012).
6. D. A. Stoyanovsky *et al*., Iron catalysis of lipid peroxidation in ferroptosis: Regulated enzymatic or random free radical reaction? *Free Radic. Biol. Med.* **133**, 153–161 (2019).
7. B. R. Stockwell *et al*., Ferroptosis: A regulated cell death nexus linking metabolism, redox biology, and disease. *Cell* **171**, 273–285 (2017).
8. S. E. Wenzel *et al*., PEBP1 wardens ferroptosis by enabling lipoxygenase generation of lipid death signals. *Cell* **171**, 628–641.e26 (2017).
9. T. S. Anthonymuthu *et al*., Empowerment of 15-lipoxygenase catalytic competence in selective oxidation of membrane ETE-PE to ferroptotic death signals, HpETE-PE. *J. Am. Chem. Soc.* **140**, 17835–17839 (2018).
10. J. P. Friedmann Angeli *et al*., Inactivation of the ferroptosis regulator Gpx4 triggers acute renal failure in mice. *Nat. Cell Biol.* **16**, 1180–1191 (2014).
11. K. Bersuker *et al*., The CoQ oxidoreductase FSP1 acts parallel to GPX4 to inhibit ferroptosis. *Nature* **575**, 688–692 (2019).
12. S. Doll *et al*., FSP1 is a glutathione-independent ferroptosis suppressor. *Nature* **575**, 693–698 (2019).
13. S. E. Ander, M. S. Diamond, C. B. Coyne, Immune responses at the maternal-fetal interface. *Sci. Immunol.* **4**, eaat6114 (2019).
14. C. P. Sibley, Treating the dysfunctional placenta. *J. Endocrinol.* **234**, R81–R97 (2017).
15. G. J. Burton, E. Jauniaux, Pathophysiology of placental-derived fetal growth restriction. *Am. J. Obstet. Gynecol.* **218**, S745–S761 (2018).
16. M. H. Schoots, S. J. Gordijn, S. A. Scherjon, H. van Goor, J. L. Hillebrands, Oxidative stress in placental pathology. *Placenta* **69**, 153–161 (2018).

17. T. Hirschhorn, B. R. Stockwell, The development of the concept of ferroptosis. *Free Radic. Biol. Med.* **133**, 130–143 (2019).
18. M. J. Soares, K. Iqbal, K. Kozai, Hypoxia and placental development. *Birth Defects Res.* **109**, 1309–1329 (2017).
19. G. J. Burton, A. L. Watson, J. Hempstock, J. N. Skepper, E. Jauniaux, Uterine glands provide histiotrophic nutrition for the human fetus during the first trimester of pregnancy. *J. Clin. Endocrinol. Metab.* **87**, 2954–2959 (2002).
20. M. Alotaibi, S. Arrowsmith, S. Wray, Hypoxia-induced force increase (HIFI) is a novel mechanism underlying the strengthening of labor contractions, produced by hypoxic stresses. *Proc. Natl. Acad. Sci. U.S.A.* **112**, 9763–9768 (2015).
21. H. S. Brar, L. D. Platt, G. R. DeVore, J. Horenstein, A. L. Medearis, Qualitative assessment of maternal uterine and fetal umbilical artery blood flow and resistance in laboring patients by Doppler velocimetry. *Am. J. Obstet. Gynecol.* **158**, 952–956 (1988).
22. T. H. Hung, J. N. Skepper, D. S. Charnock-Jones, G. J. Burton, Hypoxia-reoxygenation: A potent inducer of apoptotic changes in the human placenta and possible etiological factor in preeclampsia. *Circ. Res.* **90**, 1274–1281 (2002).
23. N. Soleymanlou *et al*., Molecular evidence of placental hypoxia in preeclampsia. *J. Clin. Endocrinol. Metab.* **90**, 4299–4308 (2005).
24. S. W. Ng, S. G. Norwitz, E. R. Norwitz, The impact of iron overload and ferroptosis on reproductive disorders in humans: Implications for preeclampsia. *Int. J. Mol. Sci.* **20**, 3283 (2019).
25. A. L. Fisher, E. Nemeth, Iron homeostasis during pregnancy. *Am. J. Clin. Nutr.* **106** (suppl. 6), 1567S–1574S (2017).
26. R. Aouache, L. Biquard, D. Vaiman, F. Miralles, Oxidative stress in preeclampsia and placental diseases. *Int. J. Mol. Sci.* **19**, 1496 (2018).
27. X. Peng *et al*., Evaluation of glutathione peroxidase 4 role in preeclampsia. *Sci. Rep.* **6**, 33300 (2016).
28. H. D. Mistry *et al*., Differential expression and distribution of placental glutathione peroxidases 1, 3 and 4 in normal and preeclamptic pregnancy. *Placenta* **31**, 401–408 (2010).
29. H. Zhang *et al*., miR-30-5p-mediated ferroptosis of trophoblasts is implicated in the pathogenesis of preeclampsia. *Redox Biol.* **29**, 101402 (2020).
30. Q. Li *et al*., Inhibition of neuronal ferroptosis protects hemorrhagic brain. *JCI Insight* **2**, e90777 (2017).
31. L. Sykes, D. A. MacIntyre, T. G. Teoh, P. R. Bennett, Anti-inflammatory prostaglandins for the prevention of preterm labour. *Reproduction* **148**, R29–R40 (2014).
32. M. Uhlén *et al*., Proteomics. Tissue-based map of the human proteome. *Science* **347**, 1260419 (2015).
33. S. Ramanadham *et al*., Calcium-independent phospholipases A2 and their roles in biological processes and diseases. *J. Lipid Res.* **56**, 1643–1668 (2015).
34. C. M. Jenkins, A. Cedars, R. W. Gross, Eicosanoid signalling pathways in the heart. *Cardiovasc. Res.* **82**, 240–249 (2009).
35. M. Strokin, M. Sergeeva, G. Reiser, Prostaglandin synthesis in rat brain astrocytes is under the control of the n-3 docosahexaenoic acid, released by group VIB calcium-independent phospholipase A2. *J. Neurochem.* **102**, 1771–1782 (2007).
36. M. A. Balboa, J. Balsinde, Oxidative stress and arachidonic acid mobilization. *Biochim. Biophys. Acta* **1761**, 385–391 (2006).
37. J. Martínez, J. J. Moreno, Role of Ca2+-independent phospholipase A2 on arachidonic acid release induced by reactive oxygen species. *Arch. Biochem. Biophys.* **392**, 257–262 (2001).
38. G. Y. Liu *et al*., The phospholipase iPLA$_2\gamma$ is a major mediator releasing oxidized aliphatic chains from cardiolipin, integrating mitochondrial bioenergetics and signaling. *J. Biol. Chem.* **292**, 10672–10684 (2017).
39. H. Song, M. Wohltmann, M. Tan, J. H. Ladenson, J. Turk, Group VIA phospholipase A2 mitigates palmitate-induced β-cell mitochondrial injury and apoptosis. *J. Biol. Chem.* **289**, 14194–14210 (2014).
40. C. Tello, A. Darling, V. Lupo, B. Pérez-Dueñas, C. Espinós, On the complexity of clinical and molecular bases of neurodegeneration with brain iron accumulation. *Clin. Genet.* **93**, 731–740 (2018).
41. M. Breitzig, C. Bhimineni, R. Lockey, N. Kolliputi, 4-Hydroxy-2-nonenal: A critical target in oxidative stress? *Am. J. Physiol. Cell Physiol.* **311**, C537–C543 (2016).
42. Y. Xie *et al*., Ferroptosis: Process and function. *Cell Death Differ.* **23**, 369–379 (2016).
43. N. Takahashi *et al*., Necrostatin-1 analogues: Critical issues on the specificity, activity and in vivo use in experimental disease models. *Cell Death Dis.* **3**, e437 (2012).
44. R. Shah, M. S. Shchepinov, D. A. Pratt, Resolving the role of lipoxygenases in the initiation and execution of ferroptosis. *ACS Cent. Sci.* **4**, 387–396 (2018).
45. S. K. Gupta, S. S. Malhotra, A. Malik, S. Verma, P. Chaudhary, Cell signaling pathways involved during invasion and syncytialization of trophoblast cells. *Am. J. Reprod. Immunol.* **75**, 361–371 (2016).
46. A. Krämer, J. Green, J. Pollard Jr., S. Tugendreich, Causal analysis approaches in ingenuity pathway analysis. *Bioinformatics* **30**, 523–530 (2014).
47. M. G. Tuuli, M. S. Longtine, D. M. Nelson, Review: Oxygen and trophoblast biology--a source of controversy. *Placenta* **32** (suppl. 2), S109–S118 (2011).
48. K. Yusuf, S. D. Smith, Y. Sadovsky, D. M. Nelson, Trophoblast differentiation modulates the activity of caspases in primary cultures of term human trophoblasts. *Pediatr. Res.* **52**, 411–415 (2002).
49. D. M. Nelson, R. D. Johnson, S. D. Smith, E. Y. Anteby, Y. Sadovsky, Hypoxia limits differentiation and up-regulates expression and activity of prostaglandin H synthase 2 in cultured trophoblast from term human placenta. *Am. J. Obstet. Gynecol.* **180**, 896–902 (1999).
50. R. Levy *et al*., Trophoblast apoptosis from pregnancies complicated by fetal growth restriction is associated with enhanced p53 expression. *Am. J. Obstet. Gynecol.* **186**, 1056–1061 (2002).
51. C. M. Jenkins, X. Han, D. J. Mancuso, R. W. Gross, Identification of calcium-independent phospholipase A2 (iPLA2) beta, and not iPLA2gamma, as the mediator of arginine vasopressin-induced arachidonic acid release in A-10 smooth muscle cells. Enantioselective mechanism-based discrimination of mammalian iPLA2s. *J. Biol. Chem.* **277**, 32807–32814 (2002).
52. E. A. Dennis, J. Cao, Y. H. Hsu, V. Magrioti, G. Kokotos, Phospholipase A2 enzymes: Physical structure, biological function, disease implication, chemical inhibition, and therapeutic intervention. *Chem. Rev.* **111**, 6130–6185 (2011).
53. L. Magtanong *et al*., Exogenous monounsaturated fatty acids promote a ferroptosis-resistant cell state. *Cell Chem. Biol.* **26**, 420–432.e9 (2019).
54. W. S. Yang *et al*., Regulation of ferroptotic cancer cell death by GPX4. *Cell* **156**, 317–331 (2014).
55. H. Imai *et al*., Early embryonic lethality caused by targeted disruption of the mouse PHGPx gene. *Biochem. Biophys. Res. Commun.* **305**, 278–286 (2003).
56. S. Gupta, A. Agarwal, R. K. Sharma, The role of placental oxidative stress and lipid peroxidation in preeclampsia. *Obstet. Gynecol. Surv.* **60**, 807–816 (2005).
57. A. Martin *et al*., Preterm birth and oxidative stress: Effects of acute physical exercise and hypoxia physiological responses. *Redox Biol.* **17**, 315–322 (2018).
58. T. A. Moore, I. M. Ahmad, M. C. Zimmerman, Oxidative stress and preterm birth: An integrative review. *Biol. Res. Nurs.* **20**, 497–512 (2018).
59. J. C. Cross, D. G. Simmons, E. D. Watson, Chorioallantoic morphogenesis and formation of the placental villous tree. *Ann. N. Y. Acad. Sci.* **995**, 84–93 (2003).
60. H. Feng, B. R. Stockwell, Unsolved mysteries: How does lipid peroxidation cause ferroptosis? *PLoS Biol.* **16**, e2006203 (2018).
61. S. Morikawa *et al*., Increased mitochondrial damage by lipid peroxidation in trophoblast cells of preeclamptic placentas. *Biochem. Mol. Biol. Int.* **41**, 767–775 (1997).
62. N. Kweider *et al*., A role for Nrf2 in redox signalling of the invasive extravillous trophoblast in severe early onset IUGR associated with preeclampsia. *PLoS One* **7**, e47055 (2012).
63. M. Khoubnasabjafari, K. Ansarin, A. Jouyban, Variations of malondialdehyde in preeclampsia. *Hypertens. Pregnancy* **35**, 346–349 (2016).
64. A. E. Consolini, M. I. Ragone, P. Bonazzola, G. A. Colareda, Mitochondrial bioenergetics during ischemia and reperfusion. *Adv. Exp. Med. Biol.* **982**, 141–167 (2017).
65. X. Fang *et al*., Ferroptosis as a target for protection against cardiomyopathy. *Proc. Natl. Acad. Sci. U.S.A.* **116**, 2672–2680 (2019).
66. Y. Yu *et al*., The ferroptosis inducer erastin enhances sensitivity of acute myeloid leukemia cells to chemotherapeutic agents. *Mol. Cell. Oncol.* **2**, e1054549 (2015).
67. K. Shimada *et al*., Global survey of cell death mechanisms reveals metabolic regulation of ferroptosis. *Nat. Chem. Biol.* **12**, 497–503 (2016).
68. F. Ursini, M. Maiorino, M. Valente, L. Ferri, C. Gregolin, Purification from pig liver of a protein which protects liposomes and biomembranes from peroxidative degradation and exhibits glutathione peroxidase activity on phosphatidylcholine hydroperoxides. *Biochim. Biophys. Acta* **710**, 197–211 (1982).
69. S. Toppo, L. Flohé, F. Ursini, S. Vanin, M. Maiorino, Catalytic mechanisms and specificities of glutathione peroxidases: Variations of a basic scheme. *Biochim. Biophys. Acta* **1790**, 1486–1500 (2009).
70. S. J. Dixon *et al*., Human haploid cell genetics reveals roles for lipid metabolism genes in nonapoptotic cell death. *ACS Chem. Biol.* **10**, 1604–1609 (2015).
71. K. J. Kinghorn *et al*., Loss of PLA2G6 leads to elevated mitochondrial lipid peroxidation and mitochondrial dysfunction. *Brain* **138**, 1801–1816 (2015).
72. C. C. Chiu *et al*., PARK14 PLA2G6 mutants are defective in preventing rotenone-induced mitochondrial dysfunction, ROS generation and activation of mitochondrial apoptotic pathway. *Oncotarget* **8**, 79046–79060 (2017).
73. Y. Zou *et al*., Cytochrome P450 oxidoreductase contributes to phospholipid peroxidation in ferroptosis. *Nat. Chem. Biol.* **16**, 302–309 (2020).
74. A. Belavgeni, S. R. Bornstein, A. Linkermann, Prominin-2 suppresses ferroptosis sensitivity. *Dev. Cell* **51**, 548–549 (2019).
75. N. Kajarabille, G. O. Latunde-Dada, Programmed cell-death by ferroptosis: Antioxidants as mitigators. *Int. J. Mol. Sci.* **20**, 4968 (2019).
76. S. M. Wyatt *et al*., The correlation between sampling site and gene expression in the term human placenta. *Placenta* **26**, 372–379 (2005).
77. H. J. Kliman, J. E. Nestler, E. Sermasi, J. M. Sanger, J. F. Strauss 3rd, Purification, characterization, and in vitro differentiation of cytotrophoblasts from human term placentae. *Endocrinology* **118**, 1567–1582 (1986).
78. J. F. Mouillet, T. Chu, D. M. Nelson, T. Mishima, Y. Sadovsky, MiR-205 silences MED1 in hypoxic primary human trophoblasts. *FASEB J.* **24**, 2030–2039 (2010).

79. E. Jauniaux, A. Watson, G. Burton, Evaluation of respiratory gases and acid-base gradients in human fetal fluids and uteroplacental tissue between 7 and 16 weeks' gestation. *Am. J. Obstet. Gynecol.* **184**, 998–1003 (2001).
80. G. J. Burton, T. Cindrova-Davies, H. W. Yung, E. Jauniaux, Oxygen and development of the human placenta. *Reproduction*, 10.1530/REP-20-0153 (2020).
81. W. T. Schaiff *et al*., Peroxisome proliferator-activated receptor-gamma modulates differentiation of human trophoblast in a ligand-specific manner. *J. Clin. Endocrinol. Metab.* **85**, 3874–3881 (2000).
82. J. Folch, M. Lees, G. H. Sloane Stanley, A simple method for the isolation and purification of total lipides from animal tissues. *J. Biol. Chem.* **226**, 497–509 (1957).
83. C. J. F. Böttcher, C. M. Van Gent, C. Pries, A rapid and sensitive sub-micro phosphorus determination. *Anal. Chim. Acta* **24**, 203–204 (1961).
84. D. Heckl *et al*., Generation of mouse models of myeloid malignancy with combinatorial genetic lesions using CRISPR-Cas9 genome editing. *Nat. Biotechnol.* **32**, 941–946 (2014).
85. A. Dobin *et al*., STAR: Ultrafast universal RNA-seq aligner. *Bioinformatics* **29**, 15–21 (2013).
86. J. Harrow *et al*., GENCODE: The reference human genome annotation for the ENCODE project. *Genome Res.* **22**, 1760–1774 (2012).
87. M. I. Love, W. Huber, S. Anders, Moderated estimation of fold change and dispersion for RNA-seq data with DESeq2. *Genome Biol.* **15**, 550 (2014).
88. National Research Council, *Guide for the Care and Use of Laboratory Animals*, (National Academies Press, Washington, DC, ed. 8, 2011).
89. G. E. Truett *et al*., Preparation of PCR-quality mouse genomic DNA with hot sodium hydroxide and tris (HotSHOT). *Biotechniques* **29**, 52-NaN, 54 (2000).